ACADEMIC PRESS

Available online at www.sciencedirect.com

SCIENCE DIRECT®

Journal of Magnetic Resonance 163 (2003) 208–214

JMR Journal of Magnetic Resonance

www.elsevier.com/locate/jmr

Sensitivity-enhanced 2D IPAP, TROSY–anti-TROSY, and E.COSY experiments: alternatives for measuring dipolar ^{15}N–$^{1}H^{N}$ couplings

Keyang Ding and Angela M. Gronenborn*

Laboratory of Chemical Physics, National Institute of Diabetes and Digestive and Kidney Diseases, National Institutes of Health, Building 5, Room 130, Bethesda, MD 20892-0520, USA

Received 17 December 2002; revised 5 March 2003

Abstract

Sensitivity-enhanced versions of the IPAP, TROSY–anti-TROSY, and E.COSY experiments for measuring one-bond ^{15}N–$^{1}H^{N}$ couplings are presented. Together with the previously developed sensitivity-enhanced E.COSY-type HSQC experiment they comprise a suite of sensitivity-enhanced experiments that allows one to chose the optimal spectrum for accurate measurement of one-bond ^{15}N–$^{1}H^{N}$ residual dipolar couplings in proteins. Since one-bond ^{15}N–$^{1}H^{N}$ residual dipolar couplings play uniquely important roles in structural NMR, these additional methods provide further tools for improving structure determination of proteins and other biological macromolecules.
Published by Elsevier Science (USA).

Keywords: Residual dipolar couplings; IPAP; TROSY–anti-TROSY; E.COSY; Sensitivity enhancement

1. Introduction

The one-bond ^{15}N–$^{1}H^{N}$ residual dipolar coupling (RDC) occupies a unique position in the arsenal of structural parameters of biological systems. In structure refinements inclusion of residual dipolar couplings imposes tight restrictions on the bond orientations and greatly improves the quality of traditional NMR structures. ^{15}N–$^{1}H^{N}$ RDCs are comparatively large, thus it is easy to obtain reliable data. In addition, measuring ^{15}N–$^{1}H^{N}$ RDCs is relatively straightforward since ^{15}N and $^{1}H^{N}$ can be treated as an isolated spin pair, if the small $^{1}H^{N}$–$^{1}H^{\alpha}$ couplings are ignored. A variety of 2D experiments [1–9] have been proposed for accurate determination of one-bond ^{15}N–$^{1}H^{N}$ dipolar couplings in proteins. All these methods fall into one of the two categories: the first one uses a quantitative *J* correlation principle [1] and in the other the couplings are directly taken from the frequency displacement [6–9]. The *J* correlation experiment is sensitive to mixing effects caused by different magnetization transfer pathways [5]. Since it involves an intensity analysis, it is also crucially dependent on the signal-to-noise ratio. The accuracy of couplings obtained by measuring peak splittings is determined by the spectral resolution and signal-to-noise ratio. Clearly, the correct peak maximum can only reliably be located if a sufficient signal-to-noise level is obtained. In practice, accuracy is most frequently compromised by low sensitivity. Therefore, sensitivity-enhanced experiments [10,11] are beneficial, while keeping the measuring time and the resulting spectral resolution unchanged.

Previously, we presented a sensitivity-enhanced E.COSY-type HSQC experiment, in which the ^{15}N–$^{1}H^{N}$ couplings were measured along the ^{1}H dimension [9]. Here, we present sensitivity-enhanced versions of the IPAP experiment [6] for measuring the splitting along the ^{15}N dimension. At the same time, sensitivity-enhanced TROSY–anti-TROSY and E.COSY experiments are presented based on a similar principle. Since in the latter the splitting can be measured along either dimension in the spectrum, they also provide a means for comparing different contributions to the extracted

* Corresponding author. Fax: +301-496-1690.
E-mail address: groneborn@nih.gov (A.M. Gronenborn).

1090-7807/$ - see front matter. Published by Elsevier Science (USA).
doi:10.1016/S1090-7807(03)00081-8

values for the two different dimensions. The sensitivity-enhanced TROSY–anti-TROSY experiment can also be used as an alternative to the sensitivity-enhanced TROSY experiment if the anti-TROSY peaks are disregarded. Together with sensitivity-enhanced E.COSY-type HSQC experiment presented earlier [9], the experiments described here provide a versatile suite of experiments from which to choose the most appropriate one for measuring one-bond ^{15}N–$^{1}H^{N}$ residual dipolar couplings in biomolecules.

2. Methods

The pulse sequence for the sensitivity-enhanced IPAP experiment is shown in Fig. 1a. The magnetization at the beginning of the evolution period t_1 can be represented by $\sigma(0) = -2H_zN_y$, where H and N represent the proton and nitrogen magnetizations, respectively. Magnetization evolves under the ^{15}N chemical shift frequency ω_N and the $^{1}H^{N}$–^{15}N coupling J_{NH} and is transformed at the end of evolution period to $\sigma(t_1)$:

$$\sigma(t_1) = [-2H_zN_y\cos(\pi J_{NH}t_1) + N_x\sin(\pi J_{NH}t_1)]\cos(\omega_N t_1) + [2H_zN_x\cos(\pi J_{NH}t_1) + N_y\sin(\pi J_{NH}t_1)]\sin(\omega_N t_1). \quad (1)$$

Table 1 lists the transformations of magnetization by the mixing pulses in the pulse sequence shown in Fig. 1a. The second term of Eq. (1) does not result in detectable magnetization and is therefore omitted in the following discussion. As can be seen from Table 1, the mixing pulses simultaneously transform $2H_zN_y$ into $-H_x$ and N_x into H_y magnetization and at the beginning of the detection period t_2, all the detectable magnetization $\sigma(t_1, 0)$ can be expressed as

$$\sigma(t_1, 0) = [H_x\cos(\pi J_{NH}t_1) + H_y\sin(\pi J_{NH}t_1)]\cos(\omega_N t_1). \quad (2)$$

In Eq. (2), the evolution of the J_{NH} coupling during t_1 is taken as the initial phase of the ^{1}H chemical shift evolution in the detection period. Therefore, the magnetization during the detection period is described by

$$\sigma(t_1, t_2) = [H_x\cos(\omega_H t_2 + \pi J_{NH}t_1) + H_y\sin(\omega_H t_2 + \pi J_{NH}t_1)]\cos(\omega_N t_1). \quad (3)$$

Inverting the sign of the phase ϕ_4 simultaneously inverts the sign of the second term in Eq. (2). This is equivalent to an inversion in sign of J_{NH} resulting in Eq. (4):

$$\sigma(t_1, t_2) = [H_x\cos(\omega_H t_2 - \pi J_{NH}t_1) + H_y\sin(\omega_H t_2 - \pi J_{NH}t_1)]\cos(\omega_N t_1). \quad (4)$$

Eqs. (3) and (4) describe the $(2n-1)$th and $(2n)$th FIDs acquired for any given t_1 increment in the 2D series. The ^{15}N chemical shift evolution in the t_1 period is always an amplitude modulation of the detected FID. After the

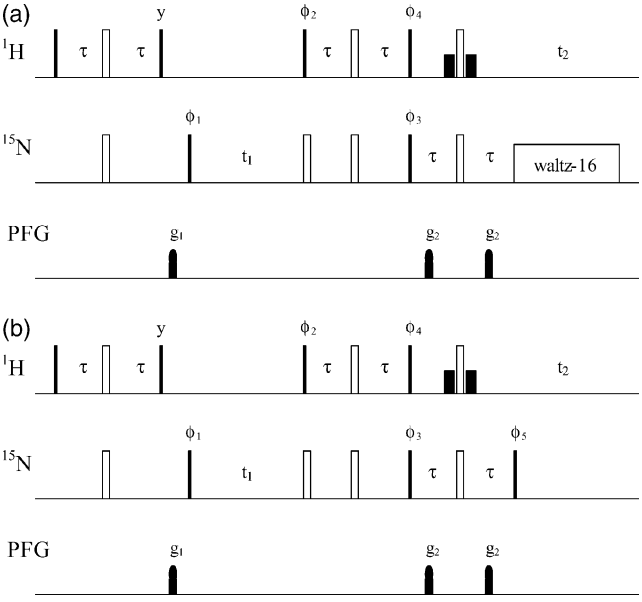

Fig. 1. Pulse sequences of sensitivity-enhanced experiments for measuring one-bond ^{15}N–$^{1}H^{N}$ couplings. Narrow (filled) and wide (open) bars represent 90° and 180° pulses with phase x, respectively, unless otherwise indicated. Watergate [16] proton 90° soft pulses of 1 ms duration are indicated by short filled bars. To decouple $^{13}C'$ and $^{13}C^{\alpha}$, π pulses (not shown) are applied at the middle of the evolution period t_1. The carrier frequencies in the ^{1}H, ^{15}N, $^{13}C'$, and $^{13}C^{\alpha}$ channels are positioned at 4.7 ppm (water resonance), 118, 177, and 56 ppm, respectively. The power level for $^{13}C'$ and $^{13}C^{\alpha}$ pulses is set at $\Delta\omega_0/(3)^{1/2}$, with $\Delta\omega_0$ the difference in Hz between the $^{13}C'$ and $^{13}C^{\alpha}$ carrier frequencies. The inter-pulse delay $\tau = 2.5$ ms. The phase ϕ_1 is incremented by 90° synchronously with incrementing t_1, which is incremented in states manner [17]. The pulse sequence in (a) describes the IPAP experiment with the following phase cycling: $\phi_1 = x, -x$; $\phi_2 = 4(x), 4(-x)$; $\phi_3 = x, x, -x, -x$; $\phi_4 = 4(y), 4(-y)$ for the $(2n-1)$th experiment and $\phi_4 = 4(-y), 4(y)$ for the $(2n)$th experiment; $\phi_{Rec} = x, -x, -x, x, -x, x, x, -x$. The pulse sequence in (b) can be used either for the TROSY–anti-TROSY or the E.COSY experiment. In the TROSY–anti-TROSY version of (b), the following phase cycling is employed: $\phi_1 = y, -y$; $\phi_2 = 4(y), 4(-y)$; $\phi_3 = y, y, -y, -y$; $\phi_4 = 4(x), 4(-x)$ for the $(2n-1)$th experiment and $\phi_4 = 4(-x), 4(x)$ for the $(2n)$th experiment, $\phi_5 = x, x, -x, -x$ for the $(2n-1)$th experiment and $\phi_5 = -x, -x, x, x$ for the $(2n)$th experiment; $\phi_{Rec} = x, -x, -x, x, -x, x, x, -x$. In the E.COSY version of (b), the phase cycling is: $\phi_1 = y, -y$; $\phi_2 = 4(y), 4(-y)$; $\phi_3 = y, y, -y, -y$; $\phi_4 = 4(-x), 4(x)$ for the $(2n-1)$th experiment and $\phi_4 = 4(x), 4(-x)$ for the $(2n)$th experiment; $\phi_5 = x, x, -x, -x$ for the $(2n-1)$th experiment and $\phi_5 = -x, -x, x, x$ for the $(2n)$th experiment; $\phi_{Rec} = x, -x, -x, x, -x, x, x, -x$. The π pulses in the $^{13}C'$ and $^{13}C^{\alpha}$ channels normally used to decouple $^{13}C'$ and $^{13}C^{\alpha}$ are omitted from the middle of the t_1 period. The PFG pulses g_1 and g_2 are sine-shaped with maximal 20 G/cm and 3 and 0.6 ms durations, respectively.

Table 1
Transformation of magnetization caused by the mixing pulses for the pulse sequence of Fig. 1a

Phases of mixing pulses	$\sigma(t_1)$	$\sigma(t_1, 0)$
$\phi_2 = x$, $\phi_4 = y$	$2H_zN_y$	$-H_x$
	N_x	H_y
	$2H_zN_x$	$-2N_xH_y$
	N_y	$-2N_xH_x$

data manipulation in echo, anti-echo manner, 2D Fourier transformation results in a 2D spectrum with cross-peaks located at (πJ_{NH}, ω_H), separated by the ^{15}N chemical shift frequency $2\omega_N$. Thus, a $^1H^N$–^{15}N doublet with individual peaks at ($\pi J_{NH} + \omega_N$, ω_H) and ($\pi J_{NH} - \omega_N$, ω_H) is observed.

The pulse sequence in Fig. 1b depicts the sensitivity-enhanced TROSY–anti-TROSY and E.COSY experiments. These two experiments differ only by a 180° phase difference for ϕ_4. The magnetization at the beginning of the evolution period t_1 is given by $\sigma(0) = 2H_zN_x = (N_x + 2H_zN_x)/2 - (N_x - 2H_zN_x)/2$, with H and N representing the proton and nitrogen magnetizations, respectively. This magnetization evolves under the ^{15}N chemical shift frequency ω_N, and the $^1H^N$–^{15}N coupling J_{NH} and is transformed at the end of evolution period to $\sigma(t_1)$:

$$\begin{aligned}\sigma(t_1) = &[(N_x + 2H_zN_x)\cos(\omega_N t_1 + \pi J_{NH} t_1)\\ &+ (N_y + 2H_zN_y)\sin(\omega_N t_1 + \pi J_{NH} t_1)]/2\\ &- [(N_x - 2H_zN_x)\cos(\omega_N t_1 - \pi J_{NH} t_1)\\ &+ (N_y - 2H_zN_y)\sin(\omega_N t_1 - \pi J_{NH} t_1)]/2. \end{aligned} \quad (5)$$

The first and second terms in Eq. (5) describe the real and imaginary parts of the high-frequency and low-frequency peaks of the J_{NH} doublet, respectively. The transformations of the magnetizations caused by the different mixing pulses are summarized in Table 2.

Applying the transformation properties listed in Table 2, the magnetization $\sigma(t_1, 0)$ at the beginning of detection period in the TROSY–anti-TROSY experiment is obtained as

$$\begin{aligned}\sigma(t_1, 0) = &[(H_y - 2N_zH_y)\cos(\omega_N t_1 + \pi J_{NH} t_1)\\ &+ (H_x - 2N_zH_x)\sin(\omega_N t_1 + \pi J_{NH} t_1)]/2\\ &+ [(H_y + 2N_zH_y)\cos(\omega_N t_1 - \pi J_{NH} t_1)\\ &- (H_x + 2N_zH_x)\sin(\omega_N t_1 - \pi J_{NH} t_1)]/2. \end{aligned} \quad (6)$$

The first term in Eq. (6) is the low-frequency peak of the J_{NH} doublet in the ^1H dimension, and the evolution of the high-frequency peak of the J_{NH} doublet in the ^{15}N dimension is taken as the initial phase in the evolution of the low-frequency peak of the J_{NH} doublet in the ^1H dimension. Similarly, the second term in Eq. (6) describes the high-frequency peak of the J_{NH} doublet in the ^1H dimension, with the evolution of the low-frequency peak of the J_{NH} doublet in the ^{15}N dimension taken as initial phase. Therefore, the detected magnetization is given by:

$$\begin{aligned}\sigma(t_1, t_2) = &\{(H_y - 2N_zH_y)\cos[(\omega_H t_2 - \pi J_{NH} t_2)\\ &- (\omega_N t_1 + \pi J_{NH} t_1)] - (H_x - 2N_zH_x)\\ &\times \sin[(\omega_H t_2 - \pi J_{NH} t_2) - (\omega_N t_1 + \pi J_{NH} t_1)]\}/2\\ &+ \{(H_y + 2N_zH_y)\cos[(\omega_H t_2 + \pi J_{NH} t_2)\\ &+ (\omega_N t_1 - \pi J_{NH} t_1)] - (H_x + 2N_zH_x)\\ &\times \sin[(\omega_H t_2 + \pi J_{NH} t_2) + (\omega_N t_1 - \pi J_{NH} t_1)]\}/2. \end{aligned} \quad (7)$$

Inversion of the phases ϕ_4 and ϕ_5 results in a change in sign for the sine terms in Eq. (6), equivalent to inverting the sign of the J_{NH} doublet peak frequencies during the t_1 period. This transforms Eq. (7) into:

$$\begin{aligned}\sigma(t_1, t_2) = &\{(H_y - 2N_zH_y)\cos[(\omega_H t_2 - \pi J_{NH} t_2)\\ &+ (\omega_N t_1 + \pi J_{NH} t_1)] - (H_x - 2N_zH_x)\\ &\times \sin[(\omega_H t_2 - \pi J_{NH} t_2) + (\omega_N t_1 + \pi J_{NH} t_1)]\}/2\\ &+ \{(H_y + 2N_zH_y)\cos[(\omega_H t_2 + \pi J_{NH} t_2)\\ &- (\omega_N t_1 - \pi J_{NH} t_1)] - (H_x + 2N_zH_x)\\ &\times \sin[(\omega_H t_2 + \pi J_{NH} t_2) - (\omega_N t_1 - \pi J_{NH} t_1)]\}/2. \end{aligned} \quad (8)$$

Eqs. (7) and (8) describe the $(2n-1)$th and $(2n)$th FIDs acquired for any given t_1 increment in the 2D series. After data manipulation in echo, anti-echo manner, 2D Fourier transformation results in a 2D spectrum with doublet cross-peaks located at ($\pi J_{NH} - \omega_N$, $\omega_H + \pi J_{NH}$) and ($\pi J_{NH} + \omega_N$, $\omega_H - \pi J_{NH}$). The cross-peaks located at ($\pi J_{NH} + \omega_N$, $\omega_H - \pi J_{NH}$) are the TROSY peaks [12], while those at ($\pi J_{NH} - \omega_N$, $\omega_H + \pi J_{NH}$) are anti-TROSY peaks.

For the E.COSY experiment, an equivalent analysis can be carried out using Table 2. In this experiment the $^1H^N$–^{15}N doublet cross-peaks are located at ($\pi J_{NH} + \omega_N$, $\omega_H + \pi J_{NH}$) and ($\pi J_{NH} - \omega_N$, $\omega_H - \pi J_{NH}$), respectively.

The implementation of the above sensitivity-enhanced experiments is carried out using a similar

Table 2
Transformation of magnetization caused by the mixing pulses for the pulse sequence of Fig. 1b

Phases of mixing pulses	$\sigma(t_1)$	$\sigma(t_1, 0)$
TROSY–anti-TROSY: $\phi_2 = y$, $\phi_4 = x$, $\phi_3 = y$, $\phi_5 = x$	$N_x + 2H_zN_x$	$H_y - 2N_zH_y$
	$N_y + 2H_zN_y$	$H_x - 2N_zH_x$
	$N_x - 2H_zN_x$	$-(H_y + 2N_zH_y)$
	$N_y - 2H_zN_y$	$H_x + 2N_zH_x$
E.COSY: $\phi_2 = y$, $\phi_4 = -x$, $\phi_3 = y$, $\phi_5 = x$	$N_x + 2H_zN_x$	$H_y + 2N_zH_y$
	$N_y + 2H_zN_y$	$-(H_x + 2N_zH_x)$
	$N_x - 2H_zN_x$	$-(H_y - 2N_zH_y)$
	$N_y - 2H_zN_y$	$-(H_x - 2N_zH_x)$

strategy as described previously [9,13]. The spectral width in the ω_1-dimension is set to be twice the ^{15}N chemical shift frequency range and an artificial ^{15}N resonance offset is achieved by using TPPI [14,15]. As in the E.COSY-type HSQC spectrum [9], the doublet peaks ($\pi J_{NH} + \omega_N$, ω_H) and ($\pi J_{NH} - \omega_N$, ω_H) in the sensitivity-enhanced IPAP spectrum, the TROSY ($\pi J_{NH} + \omega_N$, $\omega_H - \pi J_{NH}$) and anti-TROSY ($\pi J_{NH} - \omega_N$, $\omega_H + \pi J_{NH}$) peaks in the TROSY–anti-TROSY spectrum and the ($\pi J_{NH} + \omega_N$, $\omega_H + \pi J_{NH}$) and ($\pi J_{NH} - \omega_N$, $\omega_H - \pi J_{NH}$) E.COSY peaks are located in two different regions in the 2D plane governed by the sign of the ^{15}N chemical shift frequency. The resolution of these spectra is identical to that of a decoupled HSQC spectrum.

Fig. 2 displays three experimental spectra recorded using the pulse sequences illustrated in Fig. 1. The two distinct regions are easily appreciated. For example, the upper half in Fig. 2b is the TROSY spectrum and the lower half is the anti-TROSY spectrum with reversed frequency evolution in the ^{15}N dimension.

The sensitivity enhancement in the IPAP experiment for the pulse sequence in Fig. 1a is readily apparent by the following comparison. In the original IPAP scheme, two 2D data sets are recorded with spectral widths $(SW_1) \times (SW_2)$ and (NS) number of scans and (TD_1) data points in the time domain. Adding and subtracting these two data sets yields two final data sets, which are transformed into two spectra with $2(NS) \times (TD_1)$ scans in total. In the present IPAP scheme, one data set, recorded with the spectral widths $(2SW_1) \times (SW_2)$ and $(NS) \times (2TD_1)$, is transformed into a spectrum exhibiting identical resolution and sensitivity as the two spectra obtained by the original IPAP scheme, without any manipulation of the time domain data. If, however, the time domain data of the present IPAP experiment is manipulated in an echo, anti-echo manner, the resulting 2D Fourier transformation yields a 2D spectrum exhibiting identical digital resolution and 1.4 times the signal-to-noise of the original IPAP one [11,12]. The sensitivity enhancement of the TROSY–anti-TROSY and the E.COSY experiments follows accordingly. In comparison with the spin-state selective approaches [7,8], in which more than two datasets are combined together, the sensitivity enhancement of the present methods is clear, although not at first glance. Correcting for the sensitivity loss caused by cross-correlated relaxation effects results in essentially identical sensitivity for all three experiments.

Evaluation and extraction of ^{15}N–$^{1}H^{N}$ couplings along the ^{1}H dimension from the TROSY–anti-TROSY and E.COSY spectra is analogous to that for the sensitivity-enhanced E.COSY-type HSQC spectra [9]. Determination of ^{15}N–$^{1}H^{N}$ couplings along the ^{15}N dimension from these three types of spectra is depicted in Fig. 3 using the IPAP spectrum of Fig. 2a as an example. Fig. 3a is an expansion of the upper half of Fig. 2a. A second 2D Fourier transformation in reverse, or

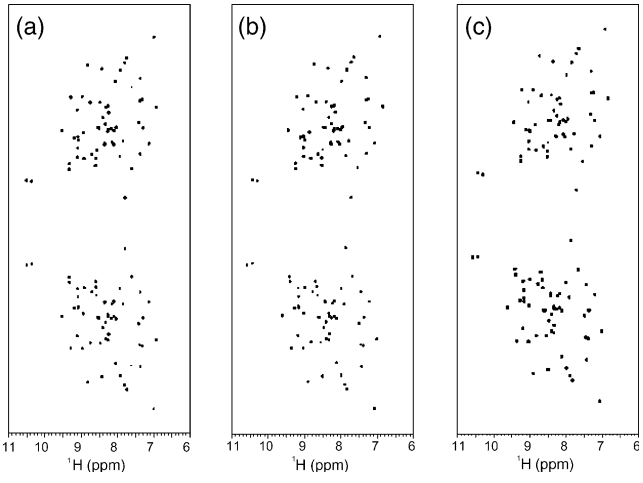

Fig. 2. Experimental spectra recorded on a 1 mM sample of uniformly ^{13}C, ^{15}N labeled protein GB1 dissolved in liquid crystalline PF1 (15 mg/ml) in 95%H_2O/5%D_2O, pH 6.95 on a Bruker DMX 600 spectrometer (600.13 MHz for ^{1}H) at 25 °C. (a) Sensitivity-enhanced IPAP spectrum recorded using the pulse sequence of Fig. 1a. The ^{15}N–$^{1}H^{N}$ couplings can be extracted along the ^{15}N dimension. (b) Sensitivity-enhanced TROSY–anti-TROSY spectrum recorded using the pulse sequence in Fig. 1b. The upper half of the spectrum is identical to the sensitivity-enhanced TROSY spectrum. (c) Sensitivity-enhanced E.COSY spectrum recorded using the pulse sequence in Fig. 1b. In the latter two spectra the ^{15}N–$^{1}H^{N}$ couplings can be extracted both along the ^{15}N and ^{1}H dimensions. The 2D spectral widths were $SW_1 \times SW_2 = 5000 \times 8992.806$ Hz; the time domain data set was $TD_1 \times TD_2 = 512 \times 1024$ with zero-filling to 1024×1024; ns = 16; the window functions in both dimensions were squared sine bell; the recycle delay = 1 s. Data were processed by using nmrPipe and nmrDraw software [18].

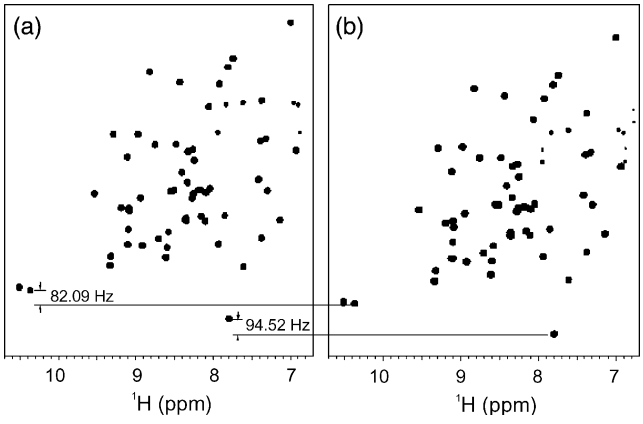

Fig. 3. Graphical illustration of extracting the ^{15}N–$^{1}H^{N}$ couplings along the ^{15}N dimension using the IPAP spectrum of Fig. 2a as the example. After 2D Fourier transformation, the upper half of the spectrum is expanded and depicted in (a). A second 2D Fourier transformation is performed on the same time-domain data set in reverse, or negative Fourier transformation in the ^{15}N dimension is carried out. The upper half of the resulting spectrum is expanded and depicted in (b). The displacement of identical cross-peaks in these two spectra yields the ^{15}N–$^{1}H^{N}$ couplings and is indicated for two individual cases.

negative Fourier transformation in the ^{15}N dimension is performed for the same time-domain data set, yielding a spectrum whose upper half is expanded and displayed in Fig. 3b. Extraction of the ^{15}N–$^{1}H^{N}$ couplings from these two expanded regions is carried out as in the original IPAP scheme, as indicated for two cross-peaks.

3. Experimental

Uniformly ^{13}C, ^{15}N labeled protein GB1 (the B1 domain of streptococcal protein G, 56 amino acids, [19]) dissolved in a colloidal suspension of 15 mg/ml Pf1 in 95% H_2O/5% D_2O, pH 6.95 was used to demonstrate the practicality of the proposed experiments. All measurements were carried out on a Bruker DMX 600 spectrometer (operating at a ^{1}H frequency of 600.13 MHz), equipped with a x,y,z-gradient triple resonance probe. All spectra were acquired at 25 °C with identical parameters: spectral widths $SW_1 \times SW_2 = 5000 \times 8992.806$ Hz; time domain data points $TD_1 \times TD_2 = 512 \times 1024$; number of scans $NS = 16$. Using a recycle delay of 1 s, each spectrum takes about 2.5 h to record.

4. Results and discussions

All three experiments (sensitivity-enhanced IPAP, TROSY–anti-TROSY, and E.COSY) were used to extract ^{15}N–$^{1}H^{N}$ RDCs for GB1. Fig. 4 illustrates the correlation between predicted ^{15}N–$^{1}H^{N}$ RDCs and measured ^{15}N–$^{1}H^{N}$ RDCs extracted from the E.COSY spectrum. Both, ^{15}N–$^{1}H^{N}$ RDCs measured along the ^{1}H or the ^{15}N dimension are examined and both exhibit excellent agreement with the predicted values. Predicted ^{15}N–$^{1}H^{N}$ RDCs were calculated based on the refined NMR structure (PDB code: 3GB1) [20] as the model using the program SSIA [21]. There is essentially no difference between the ^{15}N–$^{1}H^{N}$ RDCs from all three spectra when measured along the ^{15}N dimension. Likewise, ^{15}N–$^{1}H^{N}$ RDCs measured from TROSY–anti-TROSY and E.COSY spectra along the ^{1}H dimension are also almost identical. Interestingly though, there is a systematic difference between ^{15}N–$^{1}H^{N}$ RDCs measured along the ^{1}H and ^{15}N dimensions for the individual experiments. This can already be gleaned from Fig. 4. Comparing the absolute values of RDCs measured along the ^{1}H dimension (filled circles) with those measured along the ^{15}N dimension (open circles) reveals that the latter are always larger, a feature most clearly discernable at the extreme ends of the correlation.

This systematic difference in absolute values is illustrated vividly in Fig. 5 in which the correlation between J_{NH} values measured along the ^{15}N versus the ^{1}H dimension (A) and that between $(D+J)_{NH}$ values from

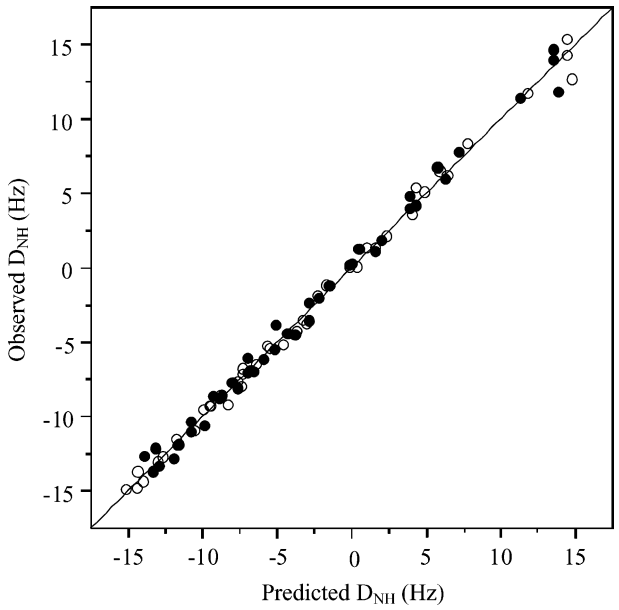

Fig. 4. Correlation between observed and predicted ^{15}N–$^{1}H^{N}$ RDCs. The experimental ^{15}N–$^{1}H^{N}$ RDCs were extracted from the E.COSY spectrum. Filled and open circles correspond to the $D_{NH}(^{1}H)$'s measured along the ^{1}H or the ^{15}N dimension, respectively. Predicted ^{15}N–$^{1}H^{N}$ RDCs were calculated using the refined NMR structure (PDB code: 3GB1) [20] as the model with the program SSIA [21]. Alignment tensor parameters employed were $D_a = 7.1$ Hz and $R = D_r/D_a = 0.659$ and $D_a = 7.7$ Hz and $R = D_r/D_a = 0.641$ for $D_{NH}(^{1}H)$ and $D_{NH}(^{15}N)$, respectively.

both dimensions (B) in TROSY–anti-TROSY and E.COSY spectra are shown, respectively. For the J_{NH} couplings, data measured along the ^{15}N dimension are systematically larger than those measured along the ^{1}H dimension. For $(D+J)_{NH}$ values there also is a systematic deviation between data measured along the ^{15}N and the ^{1}H dimension. In particular, the points for large values lie above and those for small ones lie below the diagonal line in Fig. 5b. If the splittings extracted along the ^{1}H dimension are denoted $J_{NH}(^{1}H)$ and $(D+J)_{NH}(^{1}H)$ and those along the ^{15}N dimension $J_{NH}(^{15}N)$ and $(D+J)_{NH}(^{15}N)$, respectively, the resulting differences $\Delta J_{NH} = J_{NH}(^{15}N) - J_{NH}(^{1}H)$ and $\Delta(D+J)_{NH} = (D+J)_{NH}(^{15}N) - (D+J)_{NH}(^{1}H)$ should expose any systematic bias. Comparing ΔJ_{NH} and $\Delta(D+J)_{NH}$ reveals that ΔJ_{NH} values are always positive whereas $\Delta(D+J)_{NH}$ values can exhibit positive or negative signs with no apparent correlation between them, as indicated in Fig. 6a. In contrast, the actual ^{15}N–$^{1}H^{N}$ RDCs measured along the ^{1}H and ^{15}N dimensions are highly correlated. As shown in Fig. 6b, the correlation coefficient between the ^{15}N–$^{1}H^{N}$ RDCs measured along the ^{1}H and ^{15}N dimensions is above 0.998.

The above noted systematic deviations arise from the influence of un-resolved three-bond $^{1}H^{N}$–$^{1}H^{\alpha}$ couplings and cross-correlated relaxation between ^{15}N–$^{1}H^{N}$ and $^{1}H^{N}$–$^{1}H^{\alpha}$ dipolar interactions. As shown in Fig. 7a, the

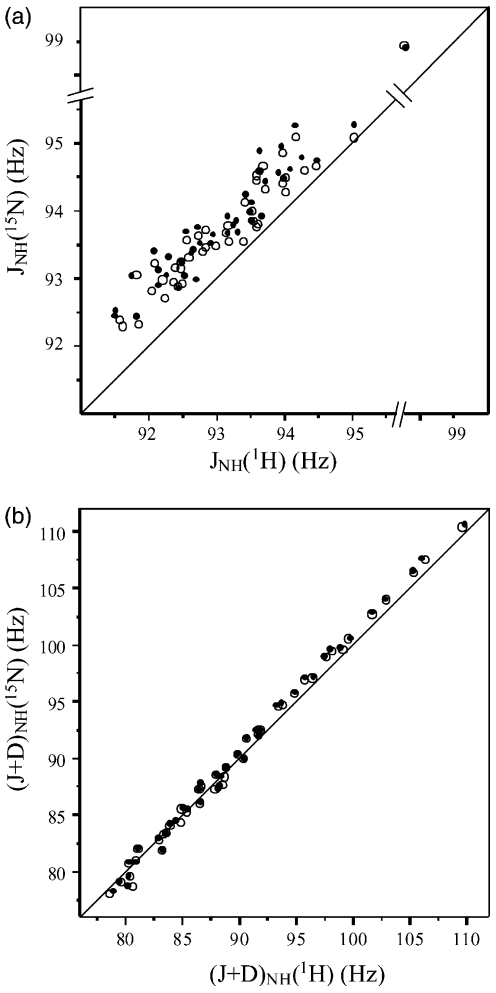

Fig. 5. Correlations between $J_{NH}(^{15}N)$ and $J_{NH}(^{1}H)$ (a) and between $(D+J)_{NH}(^{15}N)$ and $(D+J)_{NH}(^{1}H)$ (b). Filled and open circles are data obtained from the TROSY–anti-TROSY and E.COSY spectrum, respectively.

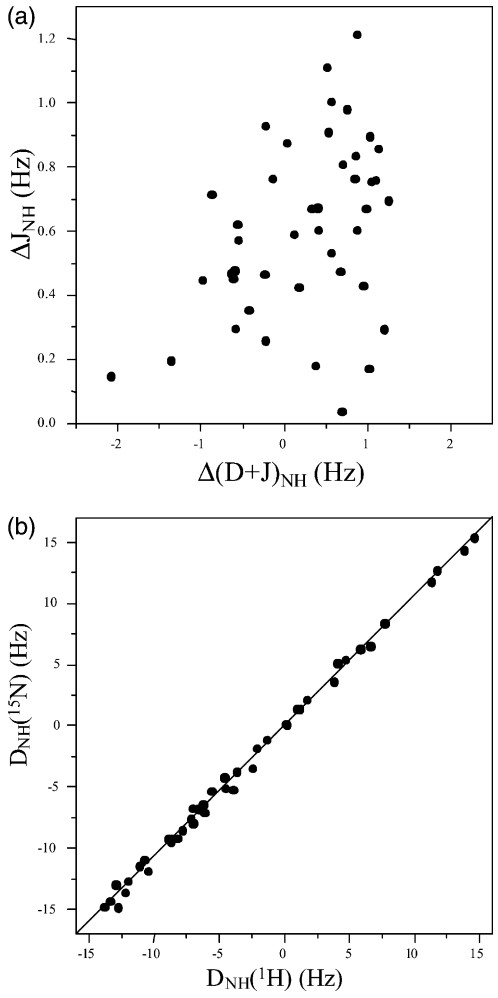

Fig. 6. (a) Correlation between ΔJ_{NH} and $\Delta(D+J)_{NH}$. ΔJ_{NH} is the difference between J_{NH} measured along the ^{15}N and ^{1}H dimensions in isotropic aqueous solution. $\Delta(D+J)_{NH}$ is the difference between $(D+J)_{NH}$ values measured along the ^{15}N and ^{1}H dimensions in an alignment medium. Thus $\Delta J_{NH} = J_{NH}(^{15}N) - J_{NH}(^{1}H)$ and $\Delta(D+J)_{NH} = (D+J)_{NH}(^{15}N) - (D+J)_{NH}(^{1}H)$. (b) Correlation between $D_{NH}(^{15}N)$ and $D_{NH}(^{1}H)$ measured from the E.COSY spectrum. $D_{NH}(^{15}N)$ and $D_{NH}(^{1}H)$ are the one-bond ^{15}N–$^{1}H^{N}$ RDCs measured along the ^{15}N and ^{1}H dimensions, respectively. The linear regression yields a slope of 1.067 with a correlation coefficient of 0.998.

distortion of the peak maximum by the three-bond coupling and the cross-correlated relaxation can be estimated by their weighted average

$$\Delta(D+J)_{NH} = {}^{3}(D+J)_{HNH\alpha} \times (I_+ - I_-)/(I_+ + I_-). \quad (9)$$

In a first approximation, the peak intensity is proportional to the reciprocal of the line width:

$$I_+ = c/[R_2(^{1}H) - \sigma] \quad \text{and} \quad I_- = c/[R_2(^{1}H) + \sigma], \quad (10)$$

with $R_2(^{1}H)$ representing the apparent ^{1}H transverse relaxation rate, σ is the cross-correlated relaxation rate between ^{15}N–$^{1}H^{N}$ and $^{1}H^{N}$–$^{1}H^{\alpha}$ dipolar interactions [22], and c a constant. Substituting Eq. (10) into Eq. (9) yields

$$\Delta(D+J)_{NH} = {}^{3}(D+J)_{HNH\alpha} \times \sigma/R_2(^{1}H). \quad (11)$$

Using Eq. (11) ΔJ_{NH} can be expressed as

$$\Delta J_{NH} = {}^{3}J_{HNH\alpha} \times \sigma/R_2(^{1}H) \quad (12)$$

and for the residual dipolar couplings, the difference $\Delta D_{NH} = D_{NH}(^{15}N) - D_{NH}(^{1}H)$ is given by

$$\Delta D_{NH} = {}^{3}D_{HNH\alpha} \times \sigma/R_2(^{1}H). \quad (13)$$

The angular part of σ is a second-order Legandre function $P_2(\cos\theta)$ of θ [22], with θ being the angle between the ^{15}N–$^{1}H^{N}$ and $^{1}H^{N}$–$^{1}H^{\alpha}$ direction and $^{3}D_{HNH\alpha}$ the axial symmetric traceless second-order tensor with its principal z-axis pointing toward the $^{1}H^{N}$–$^{1}H^{\alpha}$ distance direction. This is schematically illustrated in Fig. 7b. If D_{NH} is expressed in the principal axis system of $^{3}D_{HNH\alpha}$, an identical angular function will be obtained for Eq. (13). Therefore, $P_2(\cos\theta)$ can be viewed as a rotation between the principal axis systems of $^{3}D_{HNH\alpha}$ and D_{NH} around the x,x'-axis by the angle θ. This is equivalent to stating that the principal axis systems of the tensors ΔD_{NH} and D_{NH} coincide with each other

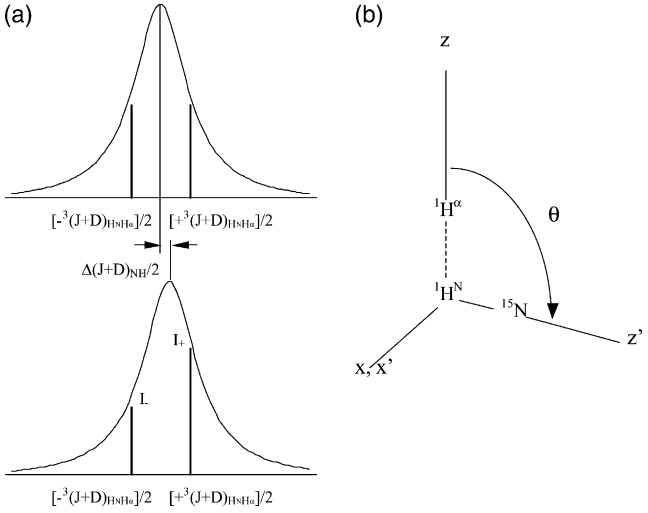

Fig. 7. (a) Illustration of the peak displacement in the ^1H dimension caused by any un-resolved three-bond $^1H^N$–$^1H^\alpha$ coupling and cross-correlated relaxation between ^{15}N–$^1H^N$ and $^1H^N$–$^1H^\alpha$ dipolar interactions. (b) The relationship between the principal axis systems of the ^{15}N–$^1H^N$ and $^1H^N$–$^1H^\alpha$ dipolar interactions.

$$\Delta D_{NH} = kD_{NH} \tag{14}$$

with the scaling factor k proportional to the reciprocal of the 6th order of $^1H^N$–$^1H^\alpha$ distance. If the $^1H^N$–$^1H^\alpha$ distances disperse over a narrow range, the ^{15}N–$^1H^N$ RDCs obtained along the ^{15}N and ^1H dimensions should only differ by this scaling factor. Therefore, both sets of RDCs should provide the correct orientations of the ^{15}N–$^1H^N$ vectors for structure determination. In addition, using the absolute values of the doublet splittings allows one to extract ΔJ_{NH} thereby providing an easy way to measure cross-correlated relaxation rates between ^{15}N–$^1H^N$ and $^1H^N$–$^1H^\alpha$ dipolar interactions.

In summary, we presented a suite of sensitivity-enhanced experiments for accurate measurements of ^{15}N–$^1H^N$ residual dipolar couplings in proteins. The general principle outlined here for the sensitivity-enhanced E.COSY experiment can also be used to measure one-bond ^{15}N–$^{13}C'$ and two-bond $^1H^N$–$^{13}C'$ dipolar couplings in other, equivalent experiments. Such experiments will be described elsewhere. Since the present three experiments are modular, they can be easily modified to measure the ^{15}N transverse relaxation rates and the cross-correlated relaxation rates between ^{15}N–$^1H^N$ dipolar and ^{15}N chemical shift interactions by inserting an INEPT pulse for building-up in-phase N_x magnetization that decays during the CPMG pulse sequence before the evolution period. If TROSY–anti-TROSY and E.COSY experiments are used to measure ^{15}N–$^1H^N$ couplings, the cross-correlated relaxation rates between ^{15}N–$^1H^N$ and $^1H^N$–$^1H^\alpha$ dipolar interactions are obtained gratuitously. If only the measurement along ^{15}N dimension is desired, the sensitivity-enhanced IPAP experiment constitutes the best choice. Since the peak intensities of the doublet are very similar for the E.COSY experiment this experiment would be most suitable for larger biomolecules for which substantial TROSY effects come into play.

Acknowledgments

This work was supported in part by the Intramural AIDS Targeted Antiviral Program of the Office of the Director of the National Institutes of Health to A.M.G.

References

[1] A. Bax, G.W. Vuister, S. Grzesiek, F. Delaglio, A.C. Wang, R. Tschudin, G. Zhu, Method Enzymol. 239 (1994) 79–105.
[2] N. Tjandra, S. Grzesiek, A. Bax, J. Am. Chem. Soc. 118 (1996) 6264–6272.
[3] J.R. Tolman, J.H. Prestegard, J. Magn. Reson. B 112 (1996) 245–252.
[4] J.R. Tolman, J.H. Prestegard, J. Magn. Reson. B 112 (1996) 269–274.
[5] B. Cutting, J.R. Tolman, S. Nanchen, G. Bodenhausen, J. Biomol. NMR 23 (2002) 195–200.
[6] M. Ottiger, F. Delaglio, A. Bax, J. Magn. Reson. 131 (1998) 373–378.
[7] F. Cordier, A.J. Dingley, S. Grzesiek, J. Biomol. NMR 13 (1999) 175–180.
[8] M.H. Lerche, A. Meissner, F.M. Poulsen, O.W. Sorensen, J. Magn. Reson. 140 (1999) 259–263.
[9] K. Ding, A.M. Gronenborn, J. Magn. Reson. 158 (2002) 173–177.
[10] A.G. Palmer III, J. Cavanagh, P.E. Wright, M. Rance, J. Magn. Reson. 93 (1991) 151–170.
[11] J. Cavanagh, A.G. Palmer III, P.E. Wright, M. Rance, J. Magn. Reson. 91 (1991) 429–436.
[12] K. Pervushin, R. Riek, G. Wider, K. Wüthrich, Proc. Natl. Acad. Sci. USA 94 (1997) 12366–12371.
[13] K. Ding, A.M. Gronenborn, J. Magn. Reson. 156 (2002) 262–268.
[14] G. Drobny, A. Pines, S. Sinton, D. Weitekamp, D. Wemmer, Faraday Div. Chem. Soc. Symp. 13 (1979) 49.
[15] G. Bodenhausen, R.L. Vold, R.R. Vold, J. Magn. Reson. 37 (1980) 93–106.
[16] M. Piotto, V. Saudek, V. Sklenar, J. Biomol. NMR 2 (1992) 661–665.
[17] D.J. States, R.A. Haberkorn, D.J. Ruben, J. Magn. Reson. 48 (1982) 286–292.
[18] F. Delaglio, S. Grzesiek, G.W. Vuister, G. Zhu, J. Pferfer, A. Bax, J. Biomol. NMR 6 (1995) 277–293.
[19] A.M. Gronenborn, D.R. Filpula, N.Z. Essig, A. Achari, M. Whitlow, P.T. Wingfield, G.M. Clore, Science 253 (1991) 657–661.
[20] J. Kuszewski, A.M. Gronenborn, G.M. Clore, J. Am. Chem. Soc. 121 (1999) 2337–2338.
[21] M. Zweckstetter, A. Bax, J. Am. Chem. Soc. 122 (2000) 3791–3792.
[22] B. Reif, M. Hennig, C. Griesinger, Science 276 (1997) 1230–1233.